TREATMENT OF HIGH LEVEL WASTE ARISING FROM PYROCHEMICAL PROCESSES

A. N. LUKINYKH, A. A. LIZIN, YU.G. LAVRINOVICH,
S. V. TOMILIN, A. G. OSIPENKO, AND M. V. KORMILITSYN
Radiochemical Division, JSC "State Scientific Center –Research Institute of Atomic Reactors", 433510, Dimitrovgrad-10, Ulyanovsk region, Russia

The paper describes the JSC "SSC RIAR" research experience on management high-level waste (HLW) arising from pyrochemical processes. The laboratory investigations including simulated and real waste forms generated as a result of the experimental reprocessings of spent nuclear fuel (SNF) of fast reactors are summarized. Pyrochemical processes are characterized by a few types and a small volume of the waste, their high specific activity and, practically, absence of the liquid process HLW. The main types of solid process wastes are phosphate and oxide precipitates and spent electrolytes. the waste forms of the pyrochemical processes can be transferred into more stable chemical forms. It was experimentally established that alumofluorine-phosphate glass or a monazite-based matrix can be used for immobilization of the phosphate waste. Oxide precipitates can be immobilized into the murataite-based melted ceramics. Alumofluorine-phosphate glass or ceramics with the kosnarite and langbeinite structures can be used for immobilization of salt electrolytes.

1. Introduction

JSC "SSC RIAR" has been performing research and development activities in support of closed fuel cycle of fast reactor since the middle of 1960s [1]. Fuel cycle involves fabrication and reprocessing of SNF using pyrochemical methods of reprocessing in molten alkali metal chlorides.

At present pyrochemical methods of SNF reprocessing in molten chlorides has reached such a level in their development that makes it possible to compare their competitiveness with classic aqueous methods. Their comparative advantage lies in high inherent safety, compactness, high protectability as to nonproliferation of nuclear materials, and reduction of high level waste volume [2].

Pyrochemical process flowsheets underwent evolutionary development at a laboratory-scale level and commercialized by operating pilot MOX fuel (mixed uranium-plutonium fuel) fabrication facility as well as trial reprocessing of irradiated uranium oxide, MOX, nitride and metallic fuel. Table 1 summarizes the operating experience of the pilot MOX fuel fabrication facility as well as trial reprocessing of spent nuclear fuel and main types of radioactive waste (RW).

Considerable study has been given to release, composition and properties of high-level waste at all the stages of development and operational verification testing of production flowsheets.

The present paper describes various reprocessing methods of recyclable products and methods of HLW preparation for controlled storage based on the gained experience of JSC "SSC RIAR". Considered here is HLW produced at different stages of fuel cycle.

2. Short summary of pyrochemical process flowsheets and management of recycable products and waste

Pyrochemical processes based on the use of molten chlorides can undergo certain changes in accordance with the goals and tasks but the main operations of the process romaine unchanged. Origin and composition of initial materials to be reprocessed have an effect on

the composition and properties of the resulted waste. In terms of radiation exposure, the most challenging task is reprocessing of irradiated fuel and so the resulted waste forms are high level waste that calls for development of special management methods and immobilization techniques in order to provide their long-term geological disposal. So the present paper is focused on the experience of JSC “SSC RIAR” in field of trial reprocessing of both MOX and dense fuel (Table1). It also gives specification of radioactive waste resulted from fuel reprocessing as well as describes experiments related to their immobilization.

Year	Fuel description	Reprocessing output (fabrication)	Main RW types	References
1988-1990	MOX-fuel for the BOR-60 and BN-600 reactors	1500 kg	Americium-containing RW	[3]
1991-1992	The BN-350 reactor fuel with a burn-up of 4.5% h.a. and cooling time of 5 years	4.1 kg	Phosphate precipitates, spent electrolytes	[4]
1995	Vibropack MOX-fuel of the BOR-60 reactor with an ultra high burn-up of 21-24% h.a. and cooling period of 2-3 years	3.3 kg	Phosphate precipitates, spent electrolytes	[5]
1998-2002	MOX-fuel (34 fuel assemblies of the BOR-60 reactor and 6 fuel assemblies of the BN-600 reactor) made of weapon-grade plutonium alloy	435 kg	RW with plutonium	[6]
2010-2011	Dense metallic fuel U-Pu, U-Zr, U-Pu-Zt with sodium sub-layer and burn-up of 6-10 % h.a. and nitride fuel U-Pu-N with lead sub-layer and burn-up of 4.8% h.a.	0.6 kg	Oxide deposits, spent electrolytes	[7]

Table 1: Experience of JSC “SSC RIAR”

2.1 Summary of the MOX-fuel reprocessing process and main types of radioactive waste

Shown in Fig.1 is the flowsheet for irradiated MOX-fuel reprocessing. The reprocessing process aims at extracting plutonium from the irradiated fuel for its reutilization and removing uranium temporarily from the cycle with the bulk of fission products for storage as uranium worthiness is much lower (because the uranium in the isotope composition occurring in nature or the uranium with lower content of the fissile isotope U-235 is used).

The MOX-fuel to be reprocessed is subjected to mechanical decladding, grinding to a powder and loaded into the head device- chlorator - electrolyser. All the operations of pyroelectrochemical reprocessing are carried out in the device. The sequence of operations is as follows:

- Fuel chlorination in molten NaCl-KCl; LiCl-NaCl-KCl-CsCl;
- Electrolysis for removal of UO_2-1 with some fission products (FPs) captured by cathodic deposit;
- Precipitate crystallization of PuO_2 decontaminated from FPs and other impurities;
- Additional electrolysis for removal of UO_2-2 with deposited FPs and other impurities;
- Molten salt purification by introduction of phosphates into the melt.

The pyrochemical reprocessing flowsheet is based on the principle of the highest possible recycling of products that will allow for obtaining a product with the PuO_2 recovery rate of 99.5-99.9% and for minimizing the production of high-level waste. Cathode deposits UO_2-1 and UO_2-2, PuO_2, and phosphate precipitate are purified from the captured salts. Aqueous

solutions are evaporated, undissolved solid salts can be returned into the very beginning of the process but condensate water is reused. The PuO_2 precipitate is expected to be used for manufacturing shortened fuel rods but uranium oxides are intended for long-term storage followed by processing and uranium return into the cycle. The phosphate precipitate passes the stages of storage, immobilization and disposal. The salts can be used for several process cycles followed by their removal from the process, storage and reprocessing before disposal. Different flammable radioactive materials can be produced when the fuel regeneration facility is under operation. Among these materials are polyethylene film, cleaning waste, overalls, filters and rubber. It was proved by experiments that all these materials can be incinerated at a regular basis in molten salts. The laboratory-scale experiments made it possible to study and specify the main parameters of incineration process for pyrographite components of the chlorator – electrolyser, which reach the end of their service life. All the equipment components including claddings of fuel rods are subjected to decontamination before they are removed from the process.

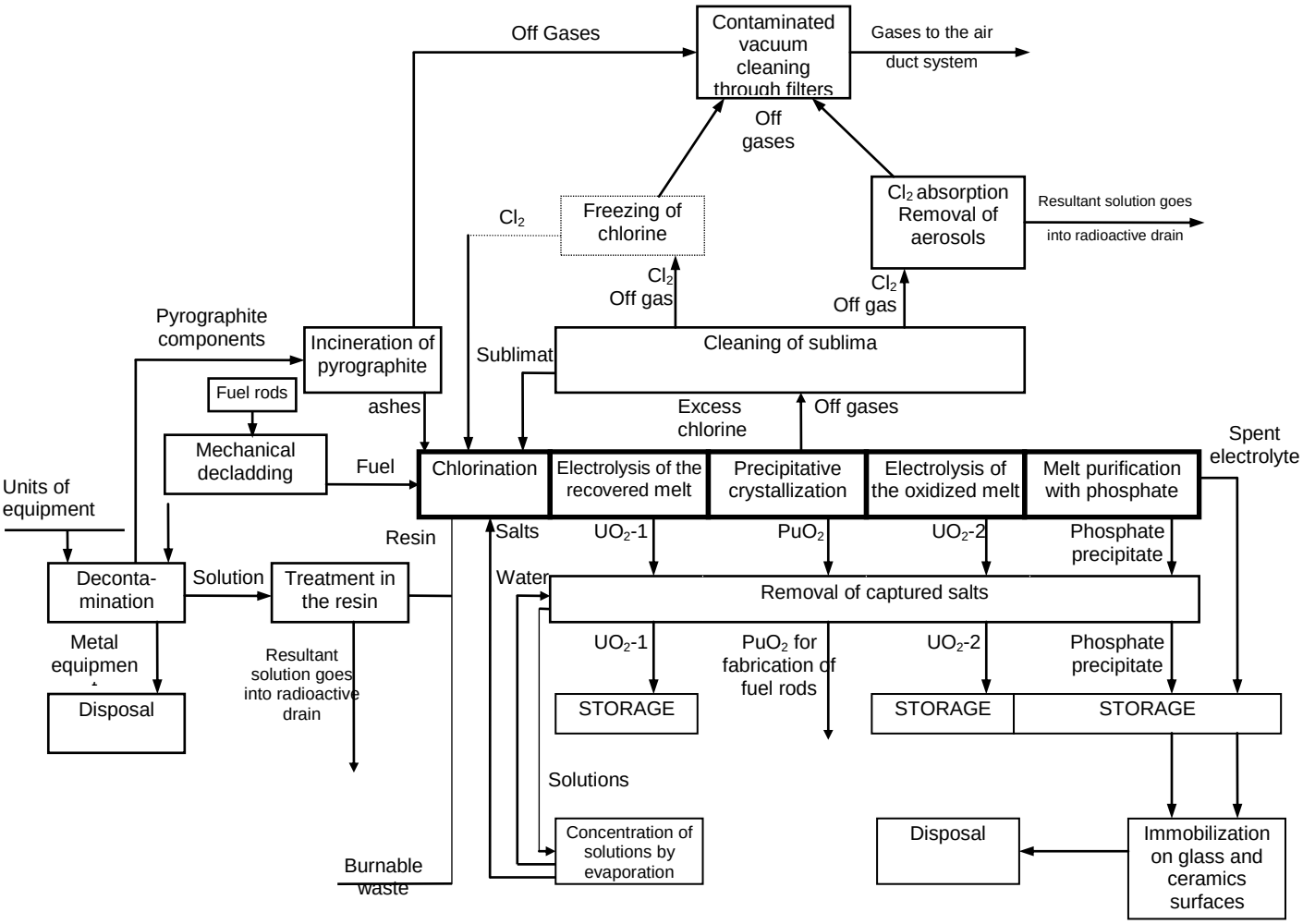

Fig 1. Integrated flowsheet of irradiated MOX-fuel reprocessing [8].

2.2 Summary of the dense SNF reprocessing process and main types of radioactive waste

In 2010-2011 the trial tests on reprocessing of dense fuel were carried out at JSC “SSC RIAR” (see Table 1). Shown in Fig.2 is the overall flowsheet of universal reprocessing for nitride and metallic fuel.

The basic processes include the following stages of the dense SNF reprocessing:

1. Regeneration through dense fuel chlorination with cadmium in molten 3LiCl-2KCl by a chemical method and electrorefining of fissile materials in a liquid cadmium cathode.
2. Elemination and condensation of liquid cadmium followed by separation fissile materials for further manufacturing of metallic and nitride fuel.
3. Partitioning of minor actinides and fission products in a liquid bismuth cathode.
4. Precipitation of fission products by introduction of carbonate followed by production, collection and removal of salts from the oxide product.
5. Immobilization of the resultant oxide product and spent electrolyte (after repeated use).

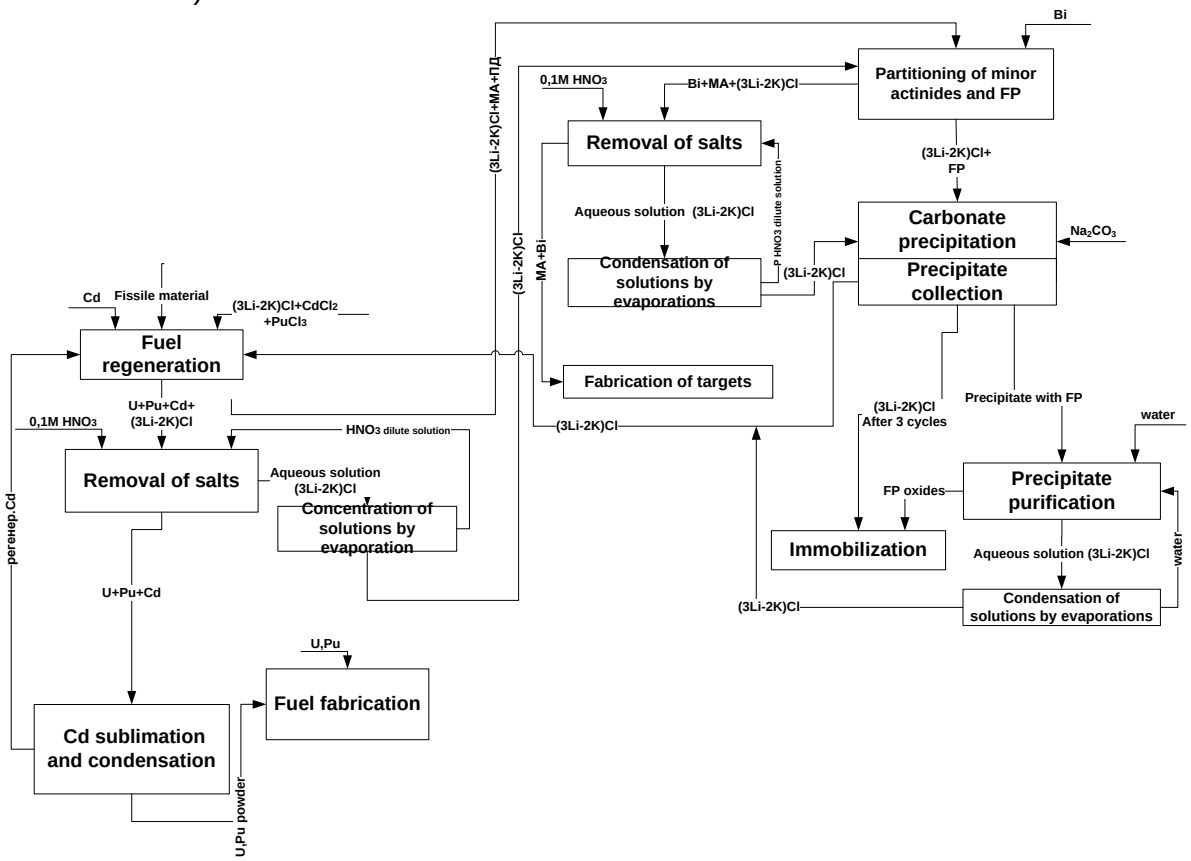

Fig 2. Integrated flowsheet of pyrochemical reprocessing of dense fuel [7]

3. HIGH LEVEL WASTE FROM PYROCHEMICAL PROCESSES AND THEIR SPECIFICATION

Certain weight quantities of HLW resulted from the experiments on reprocessing of irradiated fuel from the BN-350 and BOR-60 reactors. Experiments and studies were carried out in order to obtain physical and chemical characteristics of this waste and determine conditions of its long-term storage.

3.1 Phosphate precipitates

As a result of the BOR-60 fuel reprocessing (in 1995) phosphate precipitate was obtained. Some characteristics of this precipitate are given in Table 2. Phosphate precipitate represented itself a fine powder. It was reddish-brown in color. Nuclides ^{144}Ce + ^{144}Pr are responsible for 90% of the powder γ-activity but α-activity results from ^{241}Am by 92% (see Table 3). The X-ray diffraction analysis of the powder after annealing in air at 1000ºC revealed the presence of phase with the structure of monazite mineral i.e. (Ce, La,Y, Th…)PO_4

Under the long-term storage of HLW, the storage conditions depend largely on such properties as release of radionuclides in the environment gas as well as leachability whenever their contact with liquid phase becomes possible (for instance, with water). The

gas phase can be contaminated due to generation of radioactive aerosols and volatile chemical compounds. Leachability depends on the overall stability against solvents, especially in particular when it comes to hydrolysis. Analysis of gas phase radioactivity revealed that it depended on the $^{106}Ru+^{106}Rh$ release by 60-80%. Higher release of ^{137}Cs and ^{125}Sb was also observed. At the same time releases of ^{154}Eu and ^{155}Eu, $^{144}Ce+^{144}Pr$, and ^{241}Am are lower by 1-3 orders as opposed to Ru (Rh). It is expected that such a release occurs due to the emitted dust (sols). Probably, higher release of ruthenium radionuclides (rhodium), antimony and cesium results from higher volatility of their compounds.

Weight, g	Bulk density, g/cm^3	Specific heat release, W/kg	Specific radioactivity, Ci/g	
			α-nuclides	γ-nuclides
442	0.6-0.7	9.5	$9.3\cdot10^{-2}$	1.0

Table 2: Some characteristics of phosphate precipitate

$^{106}Ru+^{106}Rh$	$1.7\cdot10^7$	^{154}Eu	$7.8\cdot10^8$	^{241}Am	$3.2\cdot10^9$(92.5)
$^{144}Ce+^{144}Pr$	$3.3\cdot10^{10}$(90)	^{155}Eu	$0.3\cdot10^{10}$(9)	^{242}Cm	$6.3\cdot10^7$
^{137}Cs	$1.6\cdot10^7$	^{54}Mn	$4.8\cdot10^6$	^{244}Cm	$2.1\cdot10^8$
^{125}Sb	$1.3\cdot10^7$	^{60}Co	$1\cdot10^6$		

Table 3: Radioactivity of nuclides in phosphate precipitate, Bq/g (%)

Hydrolysis tests on phosphate precipitate revealed that the ^{134}Cs and ^{137}Cs isotopes make for 55% to 88% of the solution activity, the ^{144}Ce (Pr) isotopes make for 6.8% to 21% of activity and ^{125}Sb produces from 4.5% to 16% of activity (see Table 4).

Nuclides	Duration of hydrolysis tests, days				
	1	3	7	28	100
^{137}Cs	2.2	1.0	0.7	0.2	0.06
$^{144}Ce(Pr)$	$3.9\cdot10^{-4}$	$1.6\cdot10^{-4}$	$8\cdot10^{-5}$	$4.7\cdot10^{-5}$	$3.5\cdot10^{-5}$
^{125}Sb	0.1	0.07	0.07	0.03	0.02
Total of γ-nuclides	$5.3\cdot10^{-3}$	$2.3\cdot10^{-3}$	$1.7\cdot10^{-3}$	$5.3\cdot10^{-4}$	$2.1\cdot10^{-4}$
Total of α-nuclides	$2.9\cdot10^{-4}$	$7.2\cdot10^{-5}$	$5.5\cdot10^{-5}$	$2.5\cdot10^{-5}$	$2.1\cdot10^{-5}$

Table 4: Release rates of nuclides from phosphate precipitate (% as to the nuclide activity in the sample, distilled water, 20ºC).

Although $^{44}Ce+^{144}Pr$ (up to 90%) contribute to the radioactivity of phosphate precipitate to a greater degree, cesium and antimony undergo higher leaching. Probably, higher release of cesium-137 and antimony-125 from the phosphate precipitate, especially at the initial period, resulted from dissolution of residual salts as their presence was verified by thermal analysis data. As the data in table 4 suggest, the leaching rates become lower in the course of time provided that they actually take constant values in ~ a month after the beginning of test.

Test were also performed in the closed container with the phosphate precipitate (weight was 166 g, free volume- 253 cm^3) to measure a pressure. A rarefaction of $2.3\cdot10^4$ Pa (175 mm Hg) was observed in the container for 2350 h of testing at a cumulative irradiation dose of $2.1\cdot10^7$ Gy. Ionizing radiation can cause radiation and chemical transformations followed by gas phase separation. In its turn such a process can cause pressure to increase in the container with the product remaining stored in it. A rate of pressure rise is a governing factor for sealing the container. According to [9], sealing is not allowed if pressure increases at a rate of $5.1\cdot10^3$ Pa/mo (0.05 at/mo). As equilibrium has been established and pressure rises no higher than $1\cdot10^4$ Pa (0.01 at) in overall, sealing is possible. It is quite within reason to suggest that some oxygen was absorbed and bonded chemically with phosphate powder.

An essential characteristic of waste is their heating behavior, i.e. heat stability. Waste properties and reliability of its storage can be achieved in the absence of thermo-chemical and phase transformations. Thermal analysis of phosphate precipitate (at 800ºC and less in air) revealed heat-absorbing effect at 615ºC that was related to melting of residual salts in

molten alkali chlorides. In doing so, phosphate precipitate remains to be heat resistant, at least up to 600ºC, that specifies the upper boundary of temperature range under storage.
Moreover, the temperature of waste storage depends on corrosion resistance of structural materials of the cask. Widely used carbon steel St 3 and stainless steel 12X18H10T were chosen as candidate materials for manufacturing containers. The stainless steel was proven not to undergo corrosion in the phosphate precipitate environment at a self heating temperature. As to ten point grading scale of corrosion resistance, it can be assigned to the second-the forth grade (corrosion resisting steel).

3.2 Oxide precipitate

In December 2010 26 g of oxide precipitate were obtained at JSC “SSC RIAR” as a result of dense fuel reprocessing. Its characteristics are given in Table 5.

Precipitate weight, g	Content of some components and radionuclides					
	U, mass%	Pu, mass%	^{241}Am, Bq/g	^{137}Cs, Bq/g	^{154}Eu, Bq/g	^{144}Ce, Bq/g
26	4.2	<0.001	$5.4\cdot10^{6}$	$3.1\cdot10^{4}$	$1.0\cdot10^{7}$	$8.6\cdot10^{6}$

Table 5: Characteristics of real oxide precipitate

3.2 Oxide precipitate

Spent electrolytes are generated in the course of many pyrochemical processes but they are different in radiation level depending on the type of fabricated or reprocessed fuel, fuel burnup, its cooling time, efficiency of fission products precipitation in melts and repetition in use of electrolytes.
As an example, we refer to the spent electrolyte generated after high burnup fuel reprocessing of the BOR-60 reactor (1995). As a result of reprocessing 8.1 kg of molten alkali chlorides remained. Their original composition was LiCl-4.53NaCl-4.88KCl-0.66CsCl. The specific heat release of spent electrolyte was 0.95 W/kg as of June 01 1996, a temperature of self heating was about 30ºC (weight was about 2 kg). Activity of gamma nuclides depended on Cs-137 by 84% (see Table 6). The obtained alpha spectrum included 88.7% of ^{241}Am, 4.8% of ^{242}Cm and 6.5% of^{244}Cm.

U weight%	Pu weight %	Activity of α-nuclides GBq/kg	Activity of γ-nuclides, GBq/kg							
			^{106}Ru (Rh)	^{125}Sb	^{134}Cs	^{137}Cs	^{144}Ce (Pr)	^{147}Pm	^{154}Eu	^{60}Co
<0.001	<0.001	0.2	1.9	0.7	151.7	2024	200	33.3	5.9	0.1

Table 6: Chemical and radionuclide composition of spent electrolyte

Analysis of the gas phase activity over the electrolyte (weight – 2 kg, melt, end surface- 78.5 cm^2) revealed that it depended on ^{137}Cs by ~95% which was actually equivalent of its contribution to the total activity of electrolyte. As the temperature increases from 30°C up to 300ºC, the rate of activity release increases four times roughly. It was observed that the values of activity release were comparable with or a little lower than the phosphate precipitate values. Probably, the reason is that the electrolyte is solid as opposed to powders and a chance of significant powdering is excluded.
Irradiation-induced gas release was studied in the container with electrolyte (weight- 2 kg, free volume- 72.3 cm^3, cumulative dose- $1.6\cdot10^{7}$Gy) for 2350 h. A rarefaction of $5.1\cdot10^{3}$ Pa (38 mm Hg) was observed during this time period.
Thermal analysis of spent electrolyte revealed only one heat-absorbing effect at 615ºC that was related to melting of residual salts.
Corrosion tests of steels St 3 and 12X18H10T were carried out both in “cold” solid electrolyte (20°C) and hot molten electrolyte (650°C). As investigation showed, the highest corrosion rate was observed when molten electrolyte was filled in and such an effect was produced due to a high temperature of melt. Corrosion resistance of samples corresponds to grade 4 (corrosion resisting steel) for steel St 3 and grade 2 (highly corrosion resisting steel) for steel 12X18H10T.

The precipitates resulted from SNF reprocessing are qualified as high level waste and in itself this waste is concentrates of main fission products with insufficient chemical stability. Generally speaking, spent electrolyte is a composition of salts readily soluble in water. That is why a final disposal of the both waste types calls for choosing matrices that can enable steady fixation of radionuclides. Long-term safe controlled storage of waste in leak-tight containers made of steels St 3 and 12X18H10T can be considered as a short-term measure.

3. Vitrification of HLW after pyrochemical processes

3.1 Vitrification of phosphate precipitates

Since the phosphate precipitate is in the powder form and molten salt has high solubility and they have to be disposed, an additional safety barrier should be created that is embedding them into a stable matrix, e.g. glass.

A possibility is shown to embed the phosphate precipitate in the alumofluophosphate glass. The experiment on vitrification of the phosphate precipitate containing ^{241}Am (specific activity of the phosphate precipitate is $2.8 \cdot 10^8$ Bq/g) showed a high chemical resistance of the samples ($2.8 \cdot 10^{-8}$ g/cm^2*day in a week). Its deposition for 7 years did not show any structure changes.

The real phosphate precipitate generated after BOR-60 fuel reprocessing contains 22.3% of REE and 14.7% of iron; 96% of activity is given by ^{144}Ce (Pr), while 86% of alpha-activity is given by ^{241}Am. The X-ray diffraction analysis showed that the precipitate structure corresponded to the monazite one. A composition of glass matrix and waste was selected to carry out a real experiment: ($NaPO_3$-75 %, AlF_3-10%, NaF-5 %, Al_2O_3-10%)-85%, phosphate precipitation - 15%.

At the vitrification stage (T=1000°C), the release of activity into the gas phase made up $2.8 \cdot 10^{-3}$ and $1.0 \cdot 10^{-4}$ % of the initial phosphate precipitate activity for γ - and α -emitters, respectively. Among the γ -emitters, ^{125}Sb (51.6 %) and ^{137}Cs (41.9 %) made the key contribution to the gas phase activity; as for the α-emitters, it was ^{241}Am (92 %). Thermal conductivity of the vitrified waste made up 0.8-1.1W/(m·^{0}C) at 35-300°C that was an admissible level for the phosphate glass [10, 11].

The leaching rate for Na, Al, P, F and fission products at the 28th day did not exceed $1 \cdot 10^{-6}$ g/(cm^2*day) and it decreased to $1 \cdot 10^{-7}$ – $1 \cdot 10^{-8}$ g/(cm^2*day) at the 118th day. Table 7 present results of hydrolytic resistance test of the vitrified samples with phosphate precipitate.

It was stated that during a 30year storage of the glass samples (integral dose of β, γ-emission - $9.4 \cdot 10^7$ Gy, α -$1.4 \cdot 10^{23}$ decay/m^3), there was no degradation of the hydrolytic resistance. To increase the amount of phosphate precipitate in the glass, a glass matrix was developed and tested based on lead and sodium metaphosphate.

According to ref. [12], lead phosphate has long polymer chains of phosphate groups; addition of iron shortens these chains making links between them. As a result, we have glasses with a high resistance to watery dissolution. After numerous experiments, an optimal composition of the glass matrix was generated [13], mass fraction %: $Pb(PO_3)_2$ -54, $NaPO_3$-46, in which 27.5% of the phosphate precipitate was embedded. Sodium metaphosphate was added to decrease glass melt viscosity.

Corrosion resistance of the vitrified phosphate precipitate was tested using flat samples 20×15×2mm in size made of steel St.3 and 12X18H10T with the 6th grade of finish. The test was done in the solidified glass mass at 25-300°C and during the mass pouring-in at 1000°C with its further cooling to 50°C. It was stated that as the temperature rose, corrosion of the tested materials became higher. According to the 10-grade resistance scale (GOST 1338 1968), corrosion resistance of samples made of steel 12X18H10T has grade 3 (highly resistant); corrosion resistance of samples made fro steel St.3 has grade 3 at 25°C and grade 4 (resistant) at 300°C. It was experimentally stated that essentially, corrosion of samples took place during the glass mass pouring-in. Taking into account the dynamics of the corrosion rate acceleration at the elevating temperature, the optimal casks wall temperature should not exceed 400-450°C. Steel 12X18H10T is recommended for the cask material.

Nuclides	Test duration							
	3rd day	7th day	14th day	21st day	28th day	58th day	88th day	118th day
Al	$2.1\cdot10^{-6}$	$2.2\cdot10^{-6}$	$1.5\cdot10^{-6}$	$2.3\cdot10^{-7}$	$2.4\cdot10^{-7}$	$2.7\cdot10^{-7}$	$1.0\cdot10^{-7}$	$8.9\cdot10^{-8}$
Na	$1.2\cdot10^{-5}$	$7.4\cdot10^{-6}$	$7.2\cdot10^{-6}$	$6.3\cdot10^{-6}$	$4.5\cdot10^{-6}$	$3.4\cdot10^{-6}$	$1.1\cdot10^{-6}$	$5.2\cdot10^{-7}$
P	$3.0\cdot10^{-6}$	$2.9\cdot10^{-6}$	$8.4\cdot10^{-7}$	$3.2\cdot10^{-7}$	$3.5\cdot10^{-7}$	$5.1\cdot10^{-7}$	$2.7\cdot10^{-7}$	$1.6\cdot10^{-7}$
F	$7.0\cdot10^{-}$	$6.9\cdot10^{-6}$	$5.1\cdot10^{-6}$	$4.3\cdot10^{-6}$	$2.4\cdot10^{-6}$	$1.5\cdot10^{-6}$	$7.9\cdot10^{-7}$	$7.7\cdot10^{-7}$
^{125}Sb	$6.9\cdot10^{-6}$	$2.4\cdot10^{-}$	$1.3\cdot10^{-6}$	$8.1\cdot10^{-7}$	$7.4\cdot10^{-7}$	$2.4\cdot10^{-7}$	$2.4\cdot10^{-7}$	$2.2\cdot10^{-7}$
^{137}Cs	$2.2\cdot10^{-5}$	$9.7\cdot10^{-6}$	$5.6\cdot10^{-6}$	$3.9\cdot10^{-6}$	$2.8\cdot10^{-6}$	$2.7\cdot10^{-6}$	$1.6\cdot10^{-6}$	$9\cdot10^{-7}$
$^{144}Ce(^{144}$	$1.2\cdot10^{-6}$	$1.2\cdot10^{-6}$	$4.1\cdot10^{-7}$	$3.6\cdot10^{-7}$	$2.3\cdot10^{-7}$	$6.4\cdot10^{-8}$	$3.8\cdot10^{-8}$	$2.4\cdot10^{-8}$
$^{154,155}Eu$	$1.6\cdot10^{-6}$	$1.8\cdot10^{-6}$	$6.3\cdot10^{-7}$	$5.0\cdot10^{-7}$	$4.6\cdot10^{-7}$	$1.3\cdot10^{-7}$	$7.8\cdot10^{-8}$	$4.8\cdot10^{-8}$
^{241}Am	$1.1\cdot10^{-6}$	$8.7\cdot10^{-7}$	$6.6\cdot10^{-7}$	$4.9\cdot10^{-7}$	$3.3\cdot10^{-7}$	$8.8\cdot10^{-8}$	$5.9\cdot10^{-8}$	$3.9\cdot10^{-8}$
$^{242,244}Cm$	$1.2\cdot10^{-6}$	$8.5\cdot10^{-7}$	$6.7\cdot10^{-7}$	$5.0\cdot10^{-7}$	$3.4\cdot10^{-7}$	$9.3\cdot10^{-8}$	$6.5\cdot10^{-8}$	$4.4\cdot10^{-8}$

Table 7: Rate of components leaching from radioactive glass sample P-1 with phosphate precipitate at T=20-25°C, g/(cm^2*day).

3.2 Vitrification of spent electrolytes

The pyroelectrochemical reprocessing of spent fuel uses different chloride mixtures as a salt electrolyte: NaCl·KCl, NaCl·2CsCl, (Na-Li-K-Cs)Cl [4] in different mole ratio.

It was stated that amorphous transparent glass samples can be got if the charge contains less than 8% of a chloride ion. It is partially removed when the charge is melted. Up to 5% of the chloride ion contained in the transparent samples after the treatment. Thus, depending on the atomic mass of alkali metal, the total amount of chlorides that can be introduced in the glass matrix, will make mass%: 7 - 12 % for LiCl, NaCl, KCl, up to 22 % for CsCl. To increase the mass fraction of vitrified chlorides, experiments were performed to convert chloride into metaphosphate, i.e. on of the glass charge components. This additional process allows vitrifying up to 46% of salt waste.

Four model (Table 8) and three radioactive samples were obtained. The X-ray diffraction analysis of the samples showed their high level of amorphism. As for sample P-5, an experiment was carried out to determine ^{137}Cs release into the gas phase. During the experiment, the Cs-137 release, together with off-gases, made up $1.3\cdot10^{-2}$ % from the initial amount.

The hydrolythic tests show (Table 9) that inclusion of spent electrolites into the selected glass matrix allows having a glass-like materials with a high chemical stability that is one of the most important creteria of the safe HLW storage.

Sample	$KPO_3\cdot NaPO_3$*	AlF_3	Al_2O_3	$NaPO_3$	$LiPO_3\cdot4{,}53\ NaPO_3\cdot 4{,}88\ KPO_3\cdot0{,}66\ CsPO_3$*	$NaPO_3\cdot 2CsPO_3$*	NaCl · 2 CsCl
M-4	75	20	5	-	-	-	-
M-5	-	20	5	-	75	-	-
M-6	-	15	5	20	-	60	-
M-7	-	16	4	60	-	-	20
P-3	-	20	5		75	-	-
P-4	-	15	5	20	-	60	-
P-5	-	16	4	60	-	-	20

Table 8: Composition of glass samples made from electrolytes (mass fraction of the initial components,%); *After conversion of chloride into metaphosphate

Sample	Component	Test duration, days							
		3	7	14	21	28	58	88	118
M - 4	Na	$1.9\cdot10^{-5}$	$1.2\cdot10^{-5}$	$6.2\cdot10^{-6}$	$5.5\cdot10^{-6}$	$1.8\cdot10^{-6}$	$2.5\cdot10^{-7}$	$2.5\cdot10^{-7}$	$2.4\cdot10^{-7}$
	Al	$3.3\cdot10^{-6}$	$7.8\cdot10^{-7}$	$5.3\cdot10^{-7}$	$3.0\cdot10^{-7}$	$2.6\cdot10^{-7}$	$4.3\cdot10^{-8}$	$3.6\cdot10^{-8}$	$3.3\cdot10^{-8}$
	P	$2.3\cdot10^{-6}$	$1.1\cdot10^{-6}$	$7.0\cdot10^{-7}$	$2.6\cdot10^{-7}$	$1.7\cdot10^{-7}$	$5.5\cdot10^{-8}$	$4.6\cdot10^{-8}$	$4.0\cdot10^{-8}$
	F	$1.8\cdot10^{-6}$	$1.5\cdot10^{-6}$	$1.1\cdot10^{-6}$	$5.1\cdot10^{-7}$	$4.0\cdot10^{-7}$	$1.2\cdot10^{-7}$	$9.4\cdot10^{-8}$	$9.4\cdot10^{-8}$
M - 5	Na	$8.0\cdot10^{-6}$	$5.5\cdot10^{-6}$	$4.4\cdot10^{-6}$	$3.2\cdot10^{-6}$	$2.7\cdot10^{-6}$	$8.6\cdot10^{-7}$	$5.2\cdot10^{-7}$	$5.0\cdot10^{-7}$
	Al	$4.8\cdot10^{-6}$	$1.1\cdot10^{-6}$	$9.4\cdot10^{-7}$	$6.9\cdot10^{-7}$	$3.4\cdot10^{-7}$	$3.7\cdot10^{-8}$	$3.6\cdot10^{-8}$	$3.6\cdot10^{-8}$
	P	$2.5\cdot10^{-6}$	$1.2\cdot10^{-6}$	$8.5\cdot10^{-6}$	$3.6\cdot10^{-7}$	$2.6\cdot10^{-7}$	$4.9\cdot10^{-8}$	$4.9\cdot10^{-8}$	$4.3\cdot10^{-8}$
	F	$1.8\cdot10^{-6}$	$9.1\cdot10^{-7}$	$6.3\cdot10^{-7}$	$5.2\cdot10^{-7}$	$4.5\cdot10^{-7}$	$1.2\cdot10^{-7}$	$4.8\cdot10^{-8}$	$4.9\cdot10^{-8}$
P – 3	Na	$1.3\cdot10^{-5}$	$4.2\cdot10^{-6}$	$1.5\cdot10^{-6}$	$8.3\cdot10^{-7}$	$7.7\cdot10^{-7}$	$5.2\cdot10^{-7}$	$4.2\cdot10^{-7}$	$4.2\cdot10^{-7}$
	Al	$1.7\cdot10^{-5}$	$2.5\cdot10^{-6}$	$5.6\cdot10^{-7}$	$3.2\cdot10^{-7}$	$2.8\cdot10^{-7}$	$2.1\cdot10^{-7}$	$1.0\cdot10^{-7}$	$7.9\cdot10^{-8}$
	P	$8.3\cdot10^{-7}$	$7.1\cdot10^{-7}$	$6.3\cdot10^{-7}$	$5.0\cdot10^{-7}$	$6.2\cdot10^{-8}$	$5.0\cdot10^{-8}$	$5.5\cdot10^{-8}$	$5.3\cdot10^{-8}$
	F	$1.0\cdot10^{-5}$	$4.2\cdot10^{-6}$	$3.9\cdot10^{-6}$	$2.9\cdot10^{-6}$	$2.4\cdot10^{-6}$	$9.6\cdot10^{-7}$	$9.6\cdot10$	$4.1\cdot10^{-7}$
	^{137}Cs	$1.2\cdot10^{-5}$	$1.5\cdot10^{-6}$	$1.5\cdot10^{-6}$	$8.6\cdot10^{-7}$	$8.1\cdot10^{-7}$	$5.0\cdot10^{-7}$	$4.6\cdot10^{-7}$	$4.2\cdot10^{-7}$

Table 9: Rate of glass components leaching from samples at 20-25°C, g/(cm^2·day) (chlorides conversion)

4. Ceramization of HLW after pyrochemical processes

As an alternative approach to preparation of pyrochemical wastes for disposal, a possibility of their immobilization into crystal mineral-like matrices is investigated. Monazite-based matrices were investigated for embedment of phosphate precipitates while murataite-based matrices - for embedment of oxide precipitates. In case of spent electrolytes, their chemical conversion into chemically stable orthophosphate mineral-like forms with structures phosphate sodium-zirconium (kosnarite or NZP) and langbeinite was investigated.

4.1 Ceramization of phosphate precipitates

Compaction of phosphate powder by compression and annealing makes it possible to produce ceramic blocks with the properties that meet the requirements of long-term storage or disposal.

A simulator of phosphate concentrate of pyroelectrochemical process is produced from NaCl-2CsCl melt [16]. The oxides chlorated with gaseous Cl_2 were added into the melts and precipitation of fission product simulators with the use of sodium orthophosphate was carried out. The precipitate was washed from the captured salts with 0.1 N HNO_3 solutions. The procedure for precipitate production and its chemical composition (table 10) was close to technological conditions and composition of high-level radioactive product known from the previous investigations [5].

The produced powder was compacted into pellets annealed in air at 800-1400 ^{0}C for 10-12 hours. Phase composition of products was analyzed by X-raying. Chemical composition was identified by the emission spectrum analysis and X-ray spectrum microanalysis with the use of a scanning electronic microscope (SEM). The ceramics included the main monazite-like phase with the lattice parameters of a=6,773±0,003 Å; b=6,987±0,002 Å ; c=6,435±0,002 Å ; β = 103,68±0,02 degrees.

The SEM results showed the presence of three phases in its composition: light grey, grey and dark grey (fig. 3). Mass fractions of cations together with the X-ray diffraction analysis data are evident of the following:

1. light grey dominant phase – monazite incorporating lanthanides;
2. dark grey phase – ferrous orthophosphate $FePO_4$ with isomorphic impurities - Al, Cr;
3. grey phase – Fe- and Cr-based oxide $(Fe, Cr)_2O_3$ with the hematite structure.

Leach rate values for main components of ceramics are about 10^{-6}-10^{-7} g/(cm^2·day). Taking into account the localization of the most ecologically dangerous radionuclides in the monazite phase, rather high geometrical density of ceramics (ρ = 4,35 g/cm^3, 85 % of theoretical), as well as chemical and thermal stability (up to 1400 °C), the investigated ceramics can be considered as the main promising material for future technology developments

Element	Mass fraction, %	Element	Mass fraction, %	Element	Mass fraction, %	Element	Mass fraction, %
La	2,74	Gd	0,1	Ti	0,19	Pb	0,14
Ce	4,11	Y	0,41	Mo	0,55	Ca	2,74
Pr	2,06	Al	0,20	Cu	0,14	Sr	2,80
Nd	10,27	Cr	2,03	Mn	0,27	P+O	54,17
Sm	1,37	Fe	13,70	Zn	0,21		
Eu	0,20	Ni	0,55	Mg	1,02		

Table 10 Calculated composition of phosphate precipitate

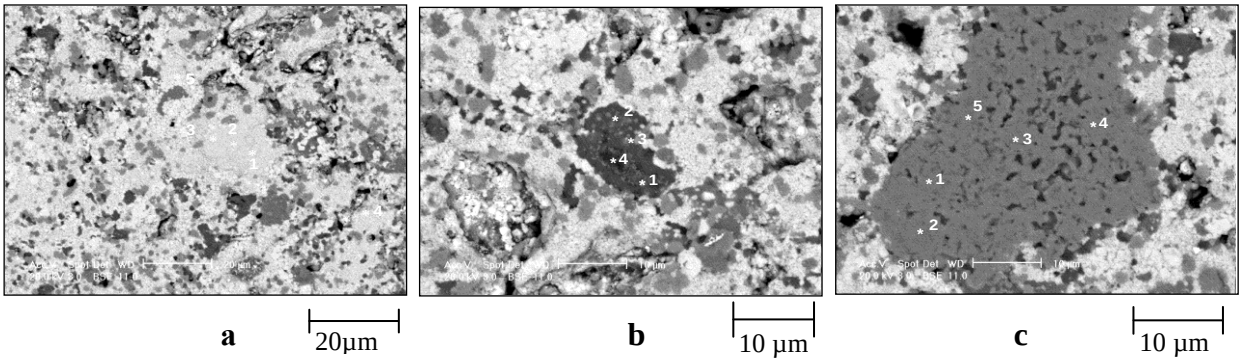

Fig 3. Images of microanalysis regions for ceramics on the basis of phosphate precipitate: light grey (a), dark grey (b) and grey (c) phases

4.2 Ceramization of oxide precipitates

To carry out the experiments on ceramization of oxide precipitates, initial charge composition developed by MosNPO RADON was taken [17]. JSC “SSC RIAR” carried out investigations on dummy and real oxide precipitates with the use of the composition presented in Table 11. Previous simulation of various ceramic compositions was performed taking into account compositions of real precipitates produced in reprocessing of dense fuel. The composition of simulated ceramics is presented in Table 11. Murataite as a dominating phase is observed for all ceramics, both fused and sintered. Figure 4 presents the X-ray diffraction pattern of fused ceramics of structure 1 and interpretation of phase composition.

Oxide	Components, mass. %	
	Composition 1	Composition 2
Charge components		
TiO_2	55	55
MnO_2	10	10
CaO	10	10
Al_2O_3	5	5
Fe_2O_3	5	5
ZrO_2	5	5
HLW simulators, 10 mass. %		
SrO	0,3934	0,0426
MoO_3	2,1930	0,2376
CeO_2	2,7222	1,8680
Pr_6O_{11}	2,5452	0,2758
Nd_2O_3	0,5042	0,0546
Sm_2O_3	0,7812	0,0846
Eu_2O_3	0,5265	0,0570
UO_2	0,3344	7,3800
	100,0001	100,0002

Table 11: Composition of produced samples of fused murataite ceramics

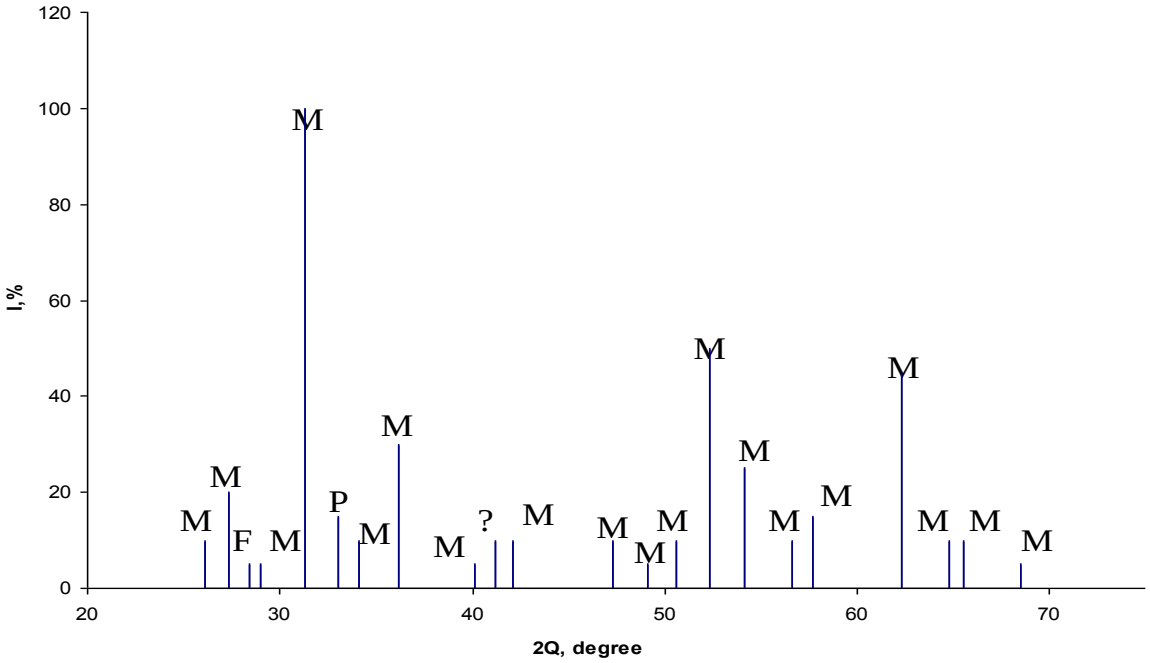

Fig 4. X-ray diffraction pattern of fused murataite ceramics (composition 1)

In the real hot experiment in the hot cell, a real oxide precipitate was used instead of simulator components. Fusion of components was conducted at 1350 ^{0}C for an hour. Figure 5 presents the high-temperature furnace in the cell and a piece of the produced fused ceramics with a real oxide precipitate

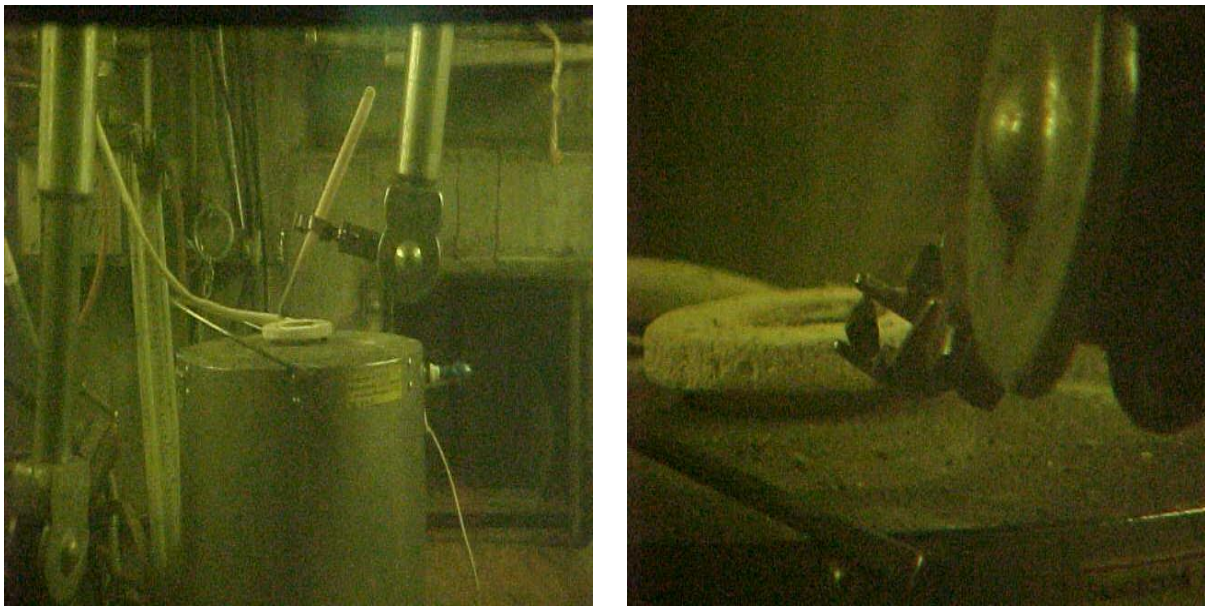

Fig 5. High-temperature furnace in the cell and a piece of produced fused ceramics with the murataite structure.

4.3 Ceramization of spent electrolytes

Orthophosphate compositions of complicated cation structure with the kosnarite mineral structure, including cations of alkaline elements from salt mixtures simulating spent chlorides of alkaline metals were produced. Their phase structure and chemical stability was investigated.

According to the reference data, in systems of double zirconium orthophosphates and cations of alkaline metals, the crystallization of the NZP-like phases depends by the nature of cations and their quantitative ratio [18, 19]. Various orthophosphate structures on the basis of electrolytes used in pyroelectrochemical process (Table 12) [20] were chosen.

Electrolyte	Orthophosphate
NaCl–KCl,	$AZr_2(PO_4)_3$ $A_3Zr_{1,5}(PO_4)_3$ $A_5Zr(PO_4)_3$
NaCl–2CsCl	$AZr_2(PO_4)_3$
LiCl–4,53NaCl– 4,88KCl–0,66CsCl	$AZr_2(PO_4)_3$ $A_3Zr_{1,5}(PO_4)_3$

Table 12: Electrolytes and corresponding orthophosphates crystallized in cosnarite structure. (A – cations of alkali metal**)**

The composition of ceramics on the kosnarite basis irrespective of a production method is formed by one or two main NZP phases. There are also phases of zirconium pyrophosphate (ZrP_2O_7) and monoclinic zirconium dioxide – brazilite (ZrO_2). At temperatures above 1300 ^{0}C the last two phases dominate (for structure of $Na_{1/3}Cs_{2/3}Zr_2(PO_4)_3$ higher than 1100^{0}C). The analysis of the crystal lattice metrics of the NZP phases showed that they represent solid solutions containing alkali cations of two or more types (Table 13).

Calculated composition	$Na_{0,5}K_{0,5}Zr_2(PO_4)_3$	$Na_{1/3}Cs_{2/3}Zr_2(PO_4)_3$	$(Li_{0,090}Na_{0,409}K_{0,441}Cs_{0,060})Zr_2(PO_4)_3$
Synthesis method	Impregnation with H_3PO_4 solution	Precipitation from solution	Precipitation from solution
Annealing	1000 ^{0}C, 3 h.	1200 ^{0}C, 5 h.	1000 ^{0}C,4 h.
Lattice parameters of the NZP phases	a = 8,737(4) Å c = 23,71(2) Å V = 1567(3) Å ^{3}	a = 8,607(3) Å c = 24,71(2) Å V = 1585(2) Å ^{3}	a = 8,746(1) Å c = 23,54(1) Å V = 1559(1) Å ^{3}

Table 13: Crystal lattice parameters for some produced phosphates with alkali metal cations.

Note: Parameter values for some orthophosphates: $LiZr_2(PO_4)_3$ (a = 8,847 Å; c = 22,24 Å, V = 1507,5 Å ^{3}), $NaZr_2(PO_4)_3$ (a = 8,804 Å ; c = 22,75 Å , V = 1527,8 Å ^{3}), $KZr_2(PO_4)_3$ (a = 8,710 Å; c = 23,89 Å, V = 1569,6 Å ^{3}), $CsZr_2(PO_4)_3$ (a = 8,580 Å ; c = 24,96 Å, V = 1591,5 Å ^{3})

The ceramics produced from the NaCl-2CsCl melt as the most widely used was subject to a more detailed research. For this purpose, microstructure, phase and chemical elemental composition were studied by SEM and X-ray spectrum microanalysis for this type of ceramics.

The analysis of backscattered electron images with composite contrast allowed to identify three main phase components of ceramics: light particles of uncertain or oblong shape, dark particles and a grey phase (fig. 6). Results of the X-ray spectrum analysis of the light and dark phase for ceramics produced from the salt system NaCl-2CsCl are evident of the existence of two phases of $Na_xCs_{1-x}Zr_2(PO_4)_3$ composition with the various content of sodium and cesium.

The main grey phase is close to the calculated chemical composition, i.e. to $Na_{0,33}Cs_{0,66}Zr_2(PO_4)_3$ and is formed by a finely-dispersed mixture of light and dark particles. Light and dark particles represent solid solutions $Na_xCs_{1-x}Zr_2(PO_4)_3$ with high enrichment in cesium and sodium, respectively. Thus, the direct proof of cesium fixture in ceramics, specifically, in the quantity corresponding to initial stoichiometry of reagents, is obtained.

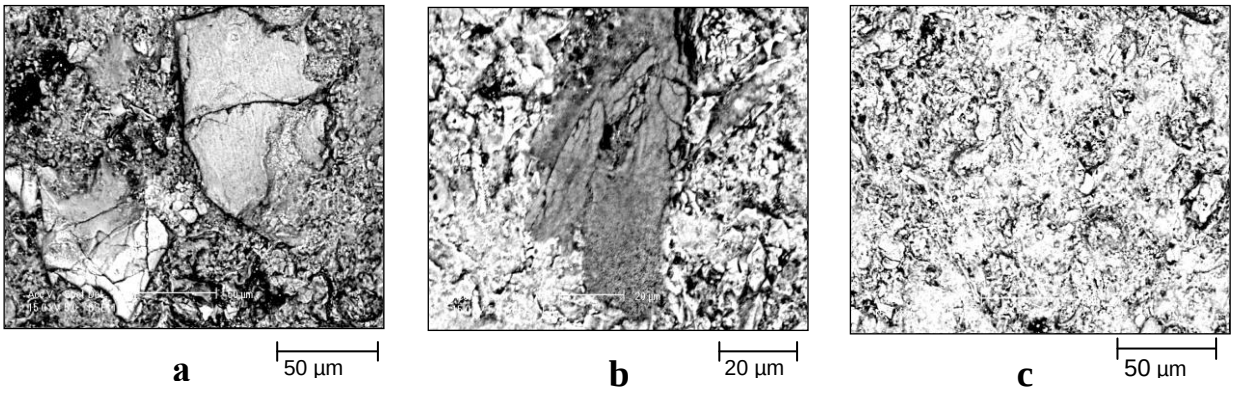

Fig 6. SEM-images of ceramic particles with the composition $Na_{1/3}Cs_{2/3}Zr_2(PO_4)_3$:
a) light phase, b) dark phase, c) grey phase

Cesium leach rates (3-14 days) were at a level of 10^{-4} g/(cm^2 ·day). These values don't correspond to permissible standards in accordance with Russian standard (GOST R 50926-96) for solidified waste forms yet. A rather high leach rate is explained by a partially loose structure of ceramics and its low density (geometrical density - 1,64 g/cm^3, theoretical one - 3,57 g/cm^3).

Therefore, to increase chemical stability and density, special processing methods were developed. To improve the ceramic material properties, washing of orthophosphate produced from the captured salts, as well as compaction and annealing with a binding material (addition of 3 % mass of 89 % Bi_2O_3+11 % NaF mixture to the press-powder) were carried out. As a result, the density of ceramics increased by 2 times, leach rate values for sodium and cesium decreased approximately by 10 times (down to 10^{-5} g/cm^2·day).

The investigations on the conversion of mixtures of alkali metal chlorides applied as electrolytes of pyrochemical processes in nuclear fuel manufacturing and reprocessing of spent nuclear fuel (SNF) into orthophosphate ceramic materials on the basis of langbeinite mineral was carried out [21]. The results of solid-phase synthesis of phosphates were described. Table 14 presents the composition of initial electrolytes and corresponding orthophosphates with the langbeinite structure produced.

Initial electrolyte	Total composition of phosphate
NaCl-KCl	$NaKFeZr(PO_4)_3$
NaCl-2CsCl	$Na_{0,66}Cs_{1,33}FeZr(PO_4)_3$
LiCl-4,53NaCl-4,88KCl-0,66CsCl	$Li_{0,18}Na_{0,82}K_{0,88}Cs_{0,12}FeZr(PO_4)_3$
NaCl-2CsCl	$Na_{0,66}Cs_{1,33}CrZr(PO_4)_3$
3LiCl-2KCl+ NaCl-2CsCl	$Li_{0,6}K_{0,4}Na_{0,33}Cs_{0,67}FeZr(PO_4)_3$

Table 14: Composition of initial electrolytes and corresponding orthophosphates with the langbeinite structure produced.

Mixtures of chlorides were subject to stepwise heat treatment at 200, 400, 600, 800 ºC with a 24-hour holding at each step and intermediate dispersion. The produced powder was compacted into pellets (diameter of a compression mold is 11 and 13 mm, compacting pressure is 150-200 MPa). Annealing of pellets was carried out at temperatures ranging within 800-1200 ^{0}C. Optimal temperatures for the formation of the langbeinite phase range within 800-950°C.

To increase the density of produced samples for the $Na_{0,66}Cs_{1,33}FeZr(PO_4)_3$ composition, a bonding agent was added (89 %Bi_2O_3 +11 %NaF mixture) in compacting ceramic pellets, total quantity being equal to 3 % of the powder initial weight. Annealing of the sample was carried out at 850ºC for 12 hours.

Ceramic samples were studied for their chemical stability (MCC-1 test, distillate, 90ºC). The materials produced with preliminary washing of powder (before compaction) from the captured chlorides and without it were investigated. The post-leaching analysis of solutions for the content of main cations was carried out by an emission-spectrum method.
For a sample with a $Na_{0,66}Cs_{1,33}FeZr(PO_4)_3$ structure, the chemical composition was quantitatively analyzed. For these purposes, scanning electronic microscopy (SEM) and X-ray spectrum microanalysis (analytical complex JSM-5300 + Link ISIS) were used. The SEM results show that the phase structure of ceramics $Na_{0,66}Cs_{1,33}FeZr(PO_4)_3$ is formed by light grey and dark grey phases (figure 7, Table 15).

Element	Mass fraction (calculation), %	Mass fraction (experiment), light grey phase, %	Mass fraction (experiment), dark grey phase, %
Na	2,45	2,06	3,59
Cs	28,37	29,52	21,13
Fe	8,94	7,04	6,87
Zr	14,61	16,47	20,19
P	14,87	14,63	16,08
O	30,74	30,16	32,14

Table 15: Calculated and experimental (X-ray spectrum microanalysis) composition of phosphate $Na_{0,66}Cs_{1,33}FeZr(PO_4)_3$

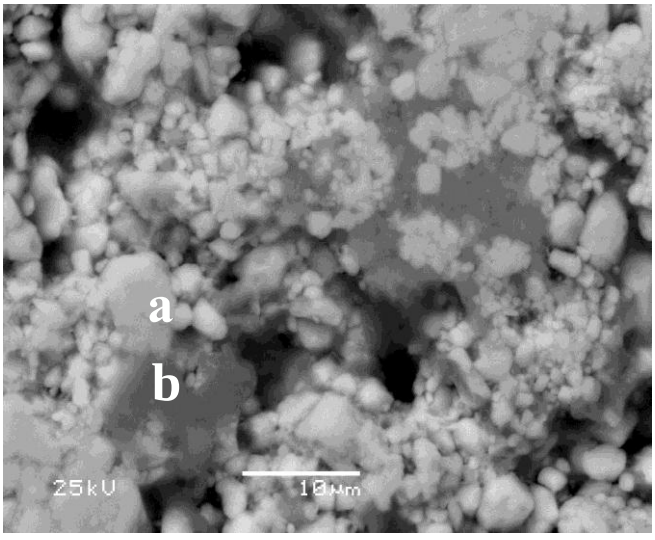

Fig 7. SEM images f ceramic particles $Na_{0,66}Cs_{1,33}FeZr(PO_4)_3$;
a-light grey phase; b- dark grey phase.

Rather good agreement of the calculated composition in synthesis of phosphate material with the data of the X-ray spectrum chemical microanalysis is observed. As a whole, the composition of both phases is close to the calculated one. A minor difference in composition of phases is that the light grey phase is a little enriched with cesium, while the dark grey one – with sodium. However, both phases belong by their structure to a langbeinite type.
Quantitative inclusion of cesium into the composition of the produced ceramic materials and stability of such compositions is experimentally shown at 800-850^{0}C. Conformity of the calculated stoichimetric composition with a real one is shown using the example of $Na_{0,66}Cs_{1,33}FeZr(PO_4)_3$.
Indicators of the chemical stability of the produced phosphates against water leaching of cations of alkali metals are by 1-2 orders higher than the required ones in accordance with

Russian GOST. Addition of a binding substance into the $Na_{0,66}Cs_{1,33}FeZr(PO_4)_3$ composition allowed to lower significantly the leaching rates of cesium (Table 16).

Element	Leaching period, days	Leaching rate, g/(cm^2·day)			
		$Na_{0,66}Cs_{1,33}FeZr(PO_4)_3$	$NaKFeZr(PO_4)_3$	$Li_{0,18}Na_{0,82}K_{0,18}Cs_{0,12}FeZr(PO_4)_3$	$Na_{0,66}Cs_{1,33}FeZr(PO_4)_3$ with binding Bi_2O_3+NaF
Na	3	$>1,1\cdot10^{-4}$	$2,3\cdot10^{-4}$	$2,9\cdot10^{-6}$	
	7	$9,8\cdot10^{-6}$	$1,0\cdot10^{-4}$	$1,7\cdot10^{-6}$	
Cs	3	$>1,1\cdot10^{-3}$		$2,3\cdot10^{-4}$	$1,4\cdot10^{-5}$
	7	$5,9\cdot10^{-4}$		$1,0\cdot10^{-4}$	$<6,4\cdot10^{-6}$
Fe	3	$3,5\cdot10^{-5}$	$3,1\cdot10^{-5}$	$3,1\cdot10^{-5}$	$6,3\cdot10^{-6}$
	7	$4,8\cdot10^{-6}$	$1,5\cdot10^{-5}$	$1,7\cdot10^{-5}$	$3,7\cdot10^{-6}$
Zr	3	$<6,6\cdot10^{-7}$	$1,6\cdot10^{-6}$	$1,0\cdot10^{-6}$	$<7,2\cdot10^{-7}$
	7	$<9,9\cdot10^{-7}$	$5,1\cdot10^{-7}$	$1,8\cdot10^{-7}$	$<6,1\cdot10^{-7}$

Table 16: Leaching rates of phosphate ceramics with the langbeinite structure

5. Conclusions

The report presents the RIAR research experience in management of high-level wastes of pyrochemical processes.

The data presented refer to the results of laboratory-scale investigations of dummy wastes, as well as of hot cell experiments with real wastes produced after pilot reprocessing of SNF from fast neutron research reactors.

Pyrochemical processes are characterized by a small spectrum and volume of the produced wastes, their high specific activity, absence of liquid high-level process wastes.

The main types of solid process wastes are phosphate and oxide precipitates, as well as spent electrolytes.

The main waste forms of pyrochemical processes can be stored long-term in shielding containers without using any schemes of their chemical conversion and immobilization.

If necessary, to enhance efficiency of the HLW shielding barrier for their long-term geological disposal, waste forms of pyrochemical processes can be converted into more stable chemical forms.

Alumofluophosphate glass and monazite-based matrix can be used for immobilization of phosphate precipitates.

Fuse ceramics on the basis of murataite mineral can be used for immobilization of oxide precipitates.

Alumofluophosphate glass and ceramics with the structures of kosnarite and langbeinite can be used for immobilization of salt electrolytes.

Further investigations on immobilization of salt systems can be aimed at a search of effective ways to prevent the formation of conversion and corrosion chlorine-containing gases, effective chemical bonding of chlorine-ion, research and development of hybrid glass-ceramic method of spent electrolytes fixation.

6. Acknowledgements

The authors are grateful to the staff of JSC “SSC RIAR”, particularly to Mr. Kayrov A.S. for the recommendations in preparation of the report concerning dense fuel processing, to Mr. Hamdeev M. I. and Mr. Baranov A. Yu. for carrying out emission spectrum and radiometric analyses, to Dr. Yakovlev V. V. and the employee of the IGEM Russian Academy of Sciences Prof. Nikonov B. S. for the help in carrying out SEM and X-ray spectrum microanalysis.

7. References

[1] Skiba et al. Technology of Pyroelectrochemical Reprocessing and Production of Nuclear Fuel./ Proc. Int. Conf. on Future Nuclear Systems: Emerging Fuel Cycles and Waste Disposal Options. GLOBAL’93. Sept. 12-17, 1993, Seattle, WA. ANS, v.2, p.1344-1350.

[2] Kirillovich et al. Safety Analisis of Fuel Cycle Processes Based on «Dry» Pyrochemical Fuel Reprocessing and Vibropac Technology./ Proc. Int. Conf. on Future Nuclear Systems. GLOBAL'97. Oct. 5-10, 1997 Pacifico Yokohama, Yokohama, Japan. Vol.2, p.900-905.
[3] Kirillovich et al. Radioactive Wastes of Fast Reactor Fuel Cycle on the Base of Dry Technologies: Properties, Handling and Reprocessing./ Proc. Int. Conf. on Future Nuclear Systems: Emerging Fuel Cycles and Waste Disposal Options. GLOBAL'93. Sept. 12-17, 1993, Seattle, WA. ANS, 1993, v.2, p.1357-1362.
[4] Bychkov et al. Pyroelectrochemical Reprocessing of Irradiated FBR MOX Fuel. Experiment on Irradiated Fuel of the BN-350 Reactor./ Proc. Int. Conf. On Evaluation of Emerging Nuclear Fuel Cycle Systems. GLOBAL'95. Sept.11-14, 1995. Versailles. v.1, p.988.
[5] Bychkov et al. Pyroelectrochemical Reprocessing of Irradiated FBR MOX Fuel. Experiment on High Burn-up Fuel of the BOR-60 Reactor./ Proc. Int. Conf. on Future Nuclear Systems. GLOBAL'97. Oct. 5-10, 1997, Pacifico Yokohama, Yokohama, Japan. Vol.2, p.912-917.
[6] Gratchyov A. F. , Skiba O. V., Tsykanov V. A. et al. Demonstration Experiment of 3 BN-600 MOX Vibropac FAs Irradiation for the Excess Weapons Plutonium Disposal // Proc. Int. Conf. on Future Nuclear Systems «GLOBAL 2005». Tsukuba, Japan, Oct 9-13, 2005 Paper № 583.
[7] Osipenko A. G., Maershin A. A., Kayrov A. S. Kormilitsyn Alexander Osipenko, Alexander Maershin, Alexey Kayrov, Mikhail Kormilitsyn. Experimental check of unified reprocessing scheme of dense spent fuel. 392274. Abstract of GLOBAL 2011. Makuhari, Japan, Dec. 11-16, 2011. p. 161.
[8] Bychkov A.V., Vavilov S.K., Porodnov P.T., Skiba O.V. Pyroelectrochemical Reprocessing of Irradiated Uranium-plutonium Oxide Fuel for Fast Neutron Reactors // Proceedings. Dimitrovgrad: SSC RIAR, 1994. Issue 1. P. 13–20.
[9] Procedure for Safe Disposal of Solidified Wastes as a Function of Properties and Specific Activity. SEV. Standing Commission on Atomic Energy Utilization in Peaceful Purposes. M., 1973.
[10] Mazurin O.V. Vitrification and Stabilization of Non-organic Glass. L.: Science, 1979.
[11] Kondratiev A.N., Kulichenko V.V, Krykov I.I. e.a. Underground Disposal of Radioactive Wastes. Vienna: IAEA, 1980. V.2, p.141.
[12] Poluektova G.B. Current Status of Issues on Management and Disposal of High-level Wastes. AINF 814. M.: TSNIIatominform, 1976.
[13] Vashman A.A., Demin A.V., Krylova N.V. et al. Phosphate Glass with Radioactive Wastes. M.: TSNIIatominform, 1977, P.172.
[14] Lavrinovich Yu.G., Kormilitsyn M.V., Konovalov V.I. et al. Vitrification of Chloride Wastes of Pyroelectrochemical Method of SNF Reprocessing. – Atomnaya Energiya, 2003,Vol.95, Issue 5, P.367-372.
[15] Lavrinovich Yu.G., Popov Yu.S., Chistyakov V.M. et al. Vitrification of Phosphate High-level Wastes Produced in Pyroelectrochemical Reprocessing of Fuel.-Proceedings. Dimitrovgrad, SSC RIAR, Issue 1, 2002. P. 59-65.
[16] Tomilin S. V., Lukinykh A. N., Lizin A. A., Bychkov A. B., Yakovlev V.V., Konovalov V.I. Investigation of Inclusion of Simulators of Fission Products and Process Impurities into Ceramics// Atomnaya Energiya. 2007. Vol. 102, №4. P. 221-224.
[17] Stefanovsky S.V., Yudintsev S.V., Omeliyanenko B.I., Nikonov B.S., Stefanovskaya O.I. Method of Immobilization of High-level Wastes into Ceramic Matrix// Patent for Invention 2 315 381. 2008, Bulletin №2.
[18] Orlova A. I., Petkov V. I., Kurazhkovskaya V. S. et al. Production and Investigation of Structure of Complex Zirconium Orthophosphates and Alkali Elements. 3. Peculiarities of Isomorphism in Li-, Na-, K-Zr-phosphates. // Radiochemistry. 1999. Vol. 41, № 4. P. 304-310.
[19] Orlova A. I., Trubach I. G., Petkov V. I. et al. Production and Investigation of Structure of Complex Zirconium Orthophosphates and Alkali Elements. 5. Phase Formation in the system of Alkali-Zirconium Phosphates of the $A_{3-x}A'_xZr_{1,5}(PO_4)_3$ (A-A$'$= Na-Li, Na-K, K-Li) type. // Radiochemistry. 2001. Vol. 43, № 3. P. 195-201.
[20] Tomilin S. V., Lukinykh A. N., Lizin A. A., Bychkov A. V., Yakovlev V. V., Konovalov V. I. Investigation on Inclusion of Spent Alkali Chloride Melts into Ceramics. // Atomnaya Energiya. 2007. Vol. 102, № 3. P. 178-182.
[21] A.A. Lizin, S. V. Tomilin, O.E. Gnevashov, A.H. Lukinykh, V. I. Konovalov. Orthophosphates with the Langbeinite Structure for Immobilization of Spent Chlorides of Pyroelectrochemical Process. // Proceedings of JSC "SSC RIAR", 2009, Issue 1-2. P.71-79.